RESIDENCE TIME MODEL

The idea of the Residence Time (RT) model is to better represent the stochastic features of turbulence when calculating the formation/depletion of pollutants. In view of it, the turbulence is represented by notional elements moving all throughout the computational domain during the calculation. The elements accumulate pollutants using the formation/depletion rates provided by the corresponding models. The resultant mean value of pollutant concentration is then obtained by summation over all elements in each computational cell. In the following, we describe the RT-model in more detail.

Initially, the computational domain is stochastically filled with a preset number of Lagrangian elements representing turbulent flow realizations. Each *i*th element is initially prescribed with its individual concentration of the *l*th pollutant Y_l^i and velocity vector u_j^i (j =1, 2, 3) which is composed of the interpolated mean value $u_{j,m}^i$ and pulsating value $u_{j,p}^i$. The letter is found using a random number generator providing a stochastic normally distributed variable.

The local instantaneous turbulence field exhibits a characteristic time $\tau = k/\varepsilon$ or frequency $\omega = 1/\tau$, where k is the local instantaneous turbulent kinetic energy and ε is its dissipation rate. This time serves as the scaling parameter for the local lifetime of turbulent eddies. Upon a time interval which exceeds the τ value considerably, the initial value of fluctuating velocity is gradually forgotten and the averaged squared velocity attains the value which is entirely determined by the turbulence and becomes independent of the initial value.

Thus, for each element we solve the equations of pollutant concentration and motion. The equation of motion contains deterministic and stochastic terms. Both deterministic and stochastic terms are constructed based on the solution of the mean flow equations.

The set of equations solved for the elements include:

Equation of motion for the ith element

$$\frac{dx_j^i}{dt} = u_j^i, \tag{1}$$

where x_j^i is the coordinate of the *i*th element (j =*1,2,3*);

Momentum conservation equation for the ith element

$$\rho^i \frac{d\vec{u_j^i}}{dt} = \frac{\partial P^i}{\partial x_j} - \nabla(pE - \tau), \tag{2}$$

where ρ^i is the material density in the *i*th element, $\nabla\tau$ is the momentum exchange term describing the effect of molecular viscosity, P^i is the mean pressure at the position of the *i*th element, p is the local instantaneous fluctuating pressure, and E is the unit matrix.

The main problem in integrating Eqs. (1) and (2) is that the second term in Eq. (2) is unknown and requires modeling. We model it in the following standard way [1]:

$$(\rho^i)^{-1}\nabla(pE - \tau) = -\zeta(u_j^i - \overline{u}_j^i) + A(t),$$

where $\overline{u}_j^i$ is the mean velocity in the point where the *i*th element is located, ζ is the coefficient ($\zeta \approx 2.075\omega$), and $A(t)$ is the stochastic function describing the variation of the pulsating velocity component in the Langevin-type equation.

Equation (2) for element velocity u_j^i can be solved separately for the "mean" $u_{j,m}^i$ and "fluctuating" $u_{j,p}^i$ velocity components. For saving the CPU time, the mean component of element velocity $u_{j,m}^i$ can be found by interpolating the mean velocity vector (provided by the CFD code) on element position. Then the motion of the *i*th element is described by two simple ordinary differential equations:

$$\frac{dx_j^i}{dt} = u_{j,m}^i + u_{j,p}^i, \tag{3}$$

$$\frac{du^i_{j,p}}{dt} = A(t) \tag{4}$$

As stated above, in the course of motion, elements accumulate pollutants according to the formation/depletion rates provided by the corresponding models. Some elements can exhibit considerably larger concentrations of pollutants than other surrounding elements. This in particular relates to those elements which move through hot recirculation zones. As a matter of fact, due to availability of molecular diffusion processes such sharp differences in pollutant concentrations cannot exist. In view of it, for each element we solve the equation of scalar transport with the chemical source term $\dot{w}$ and with the diffusion flux found based on the approximation of Linear Decay to the Mean [1]:

Equation of scalar transport

$$\frac{dY^i_l}{dt} = \dot{w}_l + C(Y^i_{l,m} - Y^i_l)\omega \tag{5}$$

where $Y^i_{l,m}$ is the local mean value of the *l*th pollutant concentration in the *i*th element, $\dot{w}_l$ is the rate of the *l*th pollutant formation/depletion, and $C \approx 2$ is the coefficient. In the RT-method, the rate $\dot{w}_l$ is found based on the mean values of species concentrations and temperature in the computational cell. Due to the second term in the RHS of Eq.(5), the arising sharp differences in the pollutant concentration in different elements somewhat smears out.

COMPUTATIONAL ALGORITHM

The algorithm of the RT-model includes the following stages:

1) Initialization of elements;
2) Moving elements at a given time step according to Eqs. (3) and (4);
3) Calculation of pollutant formation rates in each element according to Eq. (5) based on the reaction rate in the center of the corresponding computational cell;
4) Calculation of the overall pollutant formation rate by summation over all elements in cell, and
5) Calculation of new pulsating velocity component for each element, and coming back to item 2.

The algorithm has been adapted to parallel computations, unstructured computational grids with moving boundaries, rezoning, and for all available boundary conditions in AVL FIRE code [2].

NO X MODELS

It is well known that the formation of NO depends mainly on three different mechanisms, namely thermal ("Zel'dovich"), prompt ("Fenimore") and fuel NO mechanisms. Usually in automotive Diesel engine applications the third one can be neglected, because there is no significant amount of nitrogen in the fuel. The two other mechanisms can contribute to the NO formation in engines, where mainly thermal NO is formed, but also some amount of prompt NO can appear. The model used in this work, covers these two contributions [3].

THERMAL ("ZELDOVICH") NO

The thermal NO reaction mechanism is described here by the widely accepted extended Zel'dovich mechanism:

$$N_2 + O \underset{k_2}{\overset{k_1}{\leftrightarrow}} NO + N$$

$$N + O_2 \underset{k_4}{\overset{k_3}{\leftrightarrow}} NO + O$$

$$N + OH \underset{k_6}{\overset{k_5}{\leftrightarrow}} NO + H$$

It is important to point out that all three chemical reactions that represent the Zel'dovich mechanism exhibit strong temperature dependency. Derived from the above equations the overall NO formation rate $\dot{w}_{NO,Z}$ can be described as follows [4]:

$$\dot{w}_{NO,Z} = \frac{dc_{NO}}{dt} = 2k_{1f}c_O c_{N_2} \frac{\left(1 - \frac{k_{1b}k_{2b}c_{NO}^2}{k_{1f}c_{N_2}k_{2f}c_{O_2}}\right)}{1 + \frac{k_{1b}c_{NO}}{k_{2f}c_{O_2} + k_{3f}c_{OH}}} \quad (6)$$

According to these equations the thermal NO formation is independent of the fuel type. In order to solve the equations, the concentration of O atoms and the free radical OH is required which are both calculated either from empirical relations [5] or, as in the present case, based upon the radical concentrations of the ECFM-3Z combustion model [3].

PROMPT ("FENIMORE") NO

Under specific operating conditions the rate of NO generated during combustion of hydrocarbon fuel can be considerably higher than that predicted by the Zel'dovich mechanism. This enhanced NO formation is attributed to the presence of hydrocarbon species, which result from fuel fragmentation during the combustion process. Prompt ("Fenimore") NO is formed by the reaction of atmospheric nitrogen with hydrocarbon fragments, which is subsequently oxidized to form NO. The prompt NO mechanism forms NO from nitrogen much earlier in the flame than the thermal NO mechanism, as its name suggests.

The mechanism is initiated by the rapid reaction of hydrocarbon radicals with molecular nitrogen, resulting in the dissociation of N_2 and in the formation of intermediates such as HCN:

$$CH_x + N_2 \leftrightarrow HCN + N + \ldots$$

Different hydrocarbon radicals have been suggested that are responsible for prompt NO in hydrocarbon flames, but the major contribution comes from CH:

$$CH + N_2 \leftrightarrow HCN + N$$

The HCN and N then react through a series of subsequent fast reactions to form nitric oxide:

$$N + O_2 \leftrightarrow NO + O$$
$$HCN + OH \leftrightarrow CN + H_2O$$
$$CN + O_2 \leftrightarrow NO + CO$$

The model used in the present study to predict prompt NO concentration, applies an overall approximate prompt reaction proposed in [6]. A global kinetics mechanism is used to predict a rate of prompt NO, $\dot{w}_{NO,F}$:

$$\dot{w}_{NO,F} = \frac{dc_{NO}}{dt} = k_{pr}c_{O_2}^a c_{N_2} c_{fuel} \exp\left(-\frac{E}{RT}\right) \quad (7)$$

The rate of prompt NO formation is found to be of the first order with respect to nitrogen and fuel concentration, but the oxygen reaction order a depends on experimental conditions.

KINETIC SOOT MODEL

Soot formation is a complex process, which incorporates many chemical and physical steps: (1) homogeneous inception of large molecular precursors, (2) surface growth in the reactions with the gas-phase active species, (3) coalescent coagulation to form larger particles, and, finally, (4) agglomeration of the primary particles to form chain-like aggregates. The formation of molecular precursors is the first important step in the course of soot formation. Regardless the initial fuel involved, the hydrocarbon fuel undergoes either pure or oxidative pyrolysis, degrading into small hydrocarbon radicals. Under fuel-rich conditions, the small radicals react, leading to the formation of smaller hydrocarbons, particularly acetylene (C_2H_2). Then,

large hydrocarbon molecules containing a sufficiently large number of carbon atoms such as polyynes and polycyclic aromatic hydrocarbons (PAHs) are built up, that are commonly regarded as the molecular soot precursors.

For modeling soot formation in internal combustion engines using CFD software there is a need in simple and efficient soot models predicting satisfactorily the soot yield under different operation conditions. Such a model has been recently developed jointly by Semenov Institute of Chemical Physics and AVL LIST GmbH [7]. This model referred to as the Kinetic soot model includes three overall reactions:

Reaction of soot formation

$$C_nH_m + C_nH_m = 2nC + \text{Product} \qquad \text{(I)}$$

Reaction of soot oxidation by oxygen

$$C + C + O_2 = \text{Product} \qquad \text{(II)}$$

Reaction of soot oxidation by water

$$C + H_2O = \text{Product} \qquad \text{(III)}$$

where soot is represented by C atom. Since water participates in the soot oxidation reaction, the Product is attributed to either CO_2 or N_2 in order to keep minimal the number of reactive species. Each reaction is characterized by the reaction rate $\dot{w}_k$ $(k = I, II, III)$:

$$\dot{w}_k = A_k e^{-\frac{E_k}{RT}} \prod c_k$$

where T is the temperature, A_k is the preexponential factor, E_k is the activation energy, and c_k are the concentrations of species participating in the kth reaction. The rates of reactions (I), (II), and (III) are written in the form:

$$\dot{w}_I = 2nK_I c_{fuel}^2$$

$$\dot{w}_{II} = 2K_{II} c_S^2 c_{O_2}$$

$$\dot{w}_{III} = K_{III} c_S c_{H_2O}$$

where $K_k = A_k \exp(-E_k / RT)$, and c_S is the soot concentration. The kinetic parameters A_k and E_k were derived by fitting the predicted soot yields with those predicted by the detailed kinetic mechanism of soot formation and tabulated for different hydrocarbons within wide ranges of the fuel – air equivalence ratio Φ (from 1.5 to 4), pressure p (from 1 to 120 bar) and temperature T (from 1500 to 2200 K).

The detailed kinetic mechanism combines the formation mechanisms of polyaromatic hydrocarbons, polyynes, two mechanisms of soot precursor formation due to condensation of polyaromatic and polyyne molecules, soot particle growth by the reactions of HACA (Hydrogen Abstraction Carbon Addition) mechanism and polyyne molecule addition, the mechanism of acetylene pyrolysis and pure carbon cluster formation. The mechanism of *n*-tetradecane oxidation has been recently added into this detailed kinetic scheme of soot formation process. As a result, the complete detailed kinetic scheme of soot formation process incorporates over 3000 gas-phase reactions between over 300 species and 100 heterogeneous reactions with participation of four ensembles of microheterogeneous particles of different types. The rate coefficients of some important reactions have pressure dependence.

The detailed kinetic mechanism of soot formation is implemented in the MACRON code [8], which was later modified and extended [9]. In the code, formation, growth, and coagulation of soot precursors and soot particles are described within the framework of discrete Galerkin technique suggested in [10]. The technique makes it possible to preserve a discrete character of any elementary transformations of soot particles and to describe them as elementary chemical reactions for the particles of all sizes. The soot particles can also react with the gas-phase species, and thus, a connection with the detailed gas-phase chemistry of soot particles is provided during the calculation. Similar to other soot models, MACRON predictions are validated against available experimental data.

In addition to soot concentration c_S (or soot mass fraction Y_S), the MACRON code provides the complementary information on such soot parameters as particle mean diameter $\overline{D}_S$, number density n_S, and size distribution function *SDF* based on the known fuel type and the values of Φ, p, T, and overall residence time θ. This information is getting valuable in view of the forthcoming EURO-6 regulations of soot particulates. To properly utilize this information, the size distribution function *SDF* predicted by the MACRON code is approximated by the lognormal distribution:

$$SDF = \frac{n_S}{\sqrt{2\pi}\,\delta D_S} \exp\left(-\frac{\left(\ln D_S / \overline{D}_S\right)^2}{2\delta^2} \right) \tag{8}$$

where D_S is the soot particle diameter and δ is the variance of the *SDF*. Note that the values of Y_S, $\overline{D}_S$, n_S, and δ are provided by the MACRON code as functions of θ.

Soot particle parameters $\overline{D}_S$, n_S, and δ have been tabulated in the form of look-up tables using the results of detailed calculations with the MACRON code within wide ranges of Φ = 1.5–4; p = 1–120 atm; T = 1500–2200 K; and θ up to 3 ms. The soot particle parameters were shown to exhibit monotonic dependencies on Φ, p, T, and θ which guarantees acceptable interpolation accuracy between neighboring values in the look-up table. The interpolation procedure was proved to be robust and consistent. The fuel examined was n-tetradecane which is commonly used to represent Diesel oil.

As an example, Table 1 presents a fragment of the look-up table for Φ=3, p=120 atm, and T = 2200 K, whereas Figure 1 compares the size distribution functions obtained by MACRON calculations (solid red curves) with those approximated by Eq. (8) (dashed blue curves) for different residence times θ at the same values of Φ, p, and T. One can see that with time the *SDF* becomes wider and its maximum is shifted towards the larger soot particles, as could be intuitively expected. In general, the agreement between MACRON-calculated and lognormal-approximated *SDF* is seen to be satisfactory.

Thus, the Kinetic soot model coupled with the look-up tables of *SDF* parameters provides complete information on local instantaneous soot mass fraction Y_S and particle size distribution.

Table 1. Fragment of look-up tables for $\overline{D}_S$, n_S, and δ.

Φ	p, atm	T, K	θ, ms	$\overline{D}_S$, nm	n_S, 10^{13} cm^{-3}	δ
3	120	2200	0.125	10.8	2.2	0.24
			1.763	42.6	0.3	0.34
			3.000	42.7	0.2	0.38

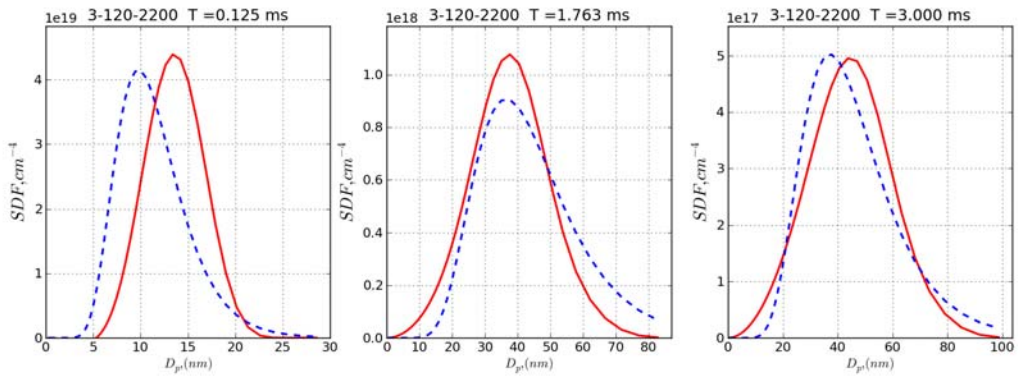

Figure 1. MACRON predicted (solid red curves) and approximated (dashed blue curves) size distribution functions at different conditions in terms of (Φ, p, T) and time θ (0.125, 1.763, and 3 ms)

ENGINE AND OPERATING CONDITIONS

The engine used for testing the RT-model is a single-cylinder research engine with electro hydraulic valve actuation and three intake ports with swirl flaps [3]. An ω-shaped piston bowl has been chosen for this study (Figure 2). The main engine and injection system data are summarized in Table 2.

The test calculations were performed for 14 engine operation points. For these points, the DoE plans were used for the design of the calculation campaign. This means that a significant number of combustion system variations have been applied by simultaneously changing the following parameters: start of injection, residual gas amount, swirl level, and injection pressure.

Computational details

All calculations were performed using AVL FIRE. In order to enable the large number of calculations of the DoE matrix to be performed within reasonable time, the calculations were done on an engine segment mesh covering 1/8 of the cylinder/piston bowl arrangement around one single fuel spray assuming cyclic symmetry. Figure 3 shows the computational grid at the crank angle 720°.

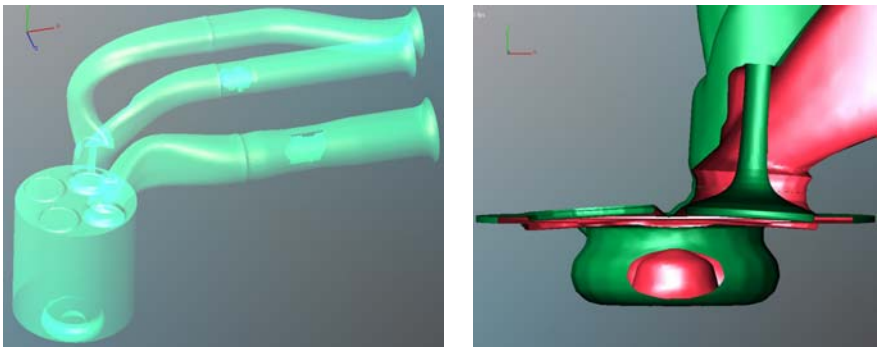

Figure 2. Engine geometry model (left), port/piston bowl configuration (right)

Table 2. Engine and injection system data [3]

Bore	85 mm
Stroke	94 mm
Displacement	533.4 cm³
Compression ratio	16:1
Injection system	BOSCH Piezo CR
Number of injection holes	8
Spray angle	158 deg

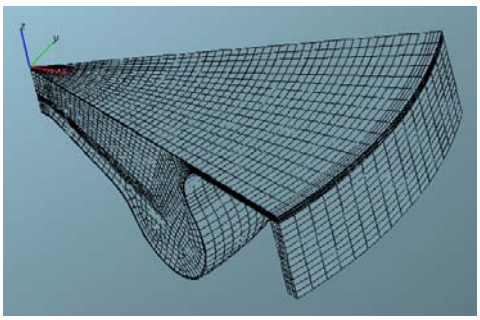

Figure 3. Computational grid.

The engine segment calculations for each DoE matrix point were started at the time of inlet valve closure (115 degree crank-angle BTDC) and commenced until opening of the exhaust valves (138 degree crank-angle ATDC). The gas side initial conditions at the time of inlet valve closure, i.e. in-cylinder pressure, temperature and residual gas mass fraction, as well as the wall temperature boundary conditions were taken from 1D cycle simulations adopting the AVL BOOST code.

A solid body rotation of the in-cylinder flow field at the time of inlet-valve closure was prescribed, with the swirl levels and turbulence intensities extracted from preceding calculations of the entire intake stroke adopting a full three-dimensional computational model.

The fuel side boundary conditions, i.e. hydraulic injection timing and injection rates for the different injection pressure levels were obtained on the basis of 1D hydraulic simulations adopting the AVL HYDSIM code. Parameterization of the hydraulic model was conducted on the basis of selected three-dimensional nozzle flow simulations.

RESULTS AND DISCUSSION

Calculations of NO formation

The results of calculations by the RT-model were compared with standard AVL FIRE results. In both cases the ECFM-3Z combustion model and the Extended Zeldovich + Prompt NO model were used. In all tests, the mean number of notional elements per cell was kept on the level of 20.

Figure 4 compares the resultant predicted NO mass fractions. Clearly, for all operation points the RT-model provides somewhat higher NO emissions.

Consider as an example the operation point #5794. As a result of calculations, we have compared the thermal NO emissions in terms of the cumulated mean mass fractions of NO as a function of crank angle (CA) predicted by the standard approach (ECFM-3Z + Extended Zel'dovich NO) and by the ECFM-3Z + Extended Zel'dovich NO + RT-model. The comparison is shown in Figure 5. Clearly, the RT-model predicts higher values of NO mass fraction evidently due to longer residence times of some elements in "hot" computational cells.

Figure 6 compares the spatial distributions of thermal NO mass fraction in the engine at different values of CA. To demonstrate the reason why the locations with high thermal NO concentration appear in

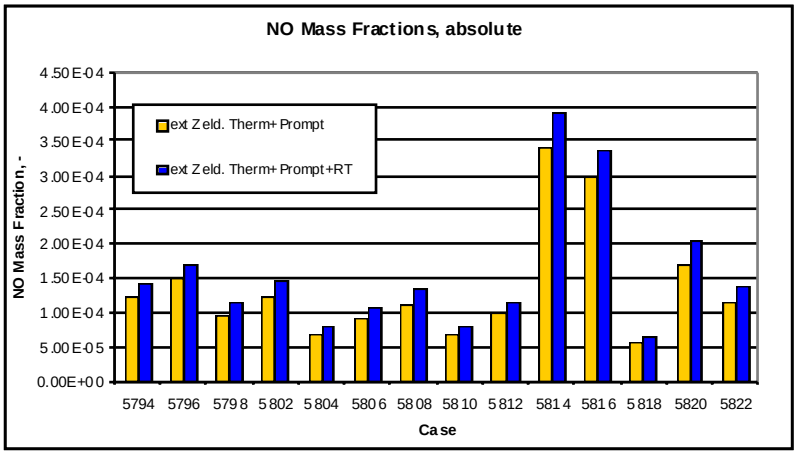

Figure 4. Comparison of NO emissions predicted by the standard ECFM-3Z + Extended Zeldovich NO + Prompt NO model (left columns marked in yellow) and the RT-model for different operation points of Diesel engine (right columns marked in blue).

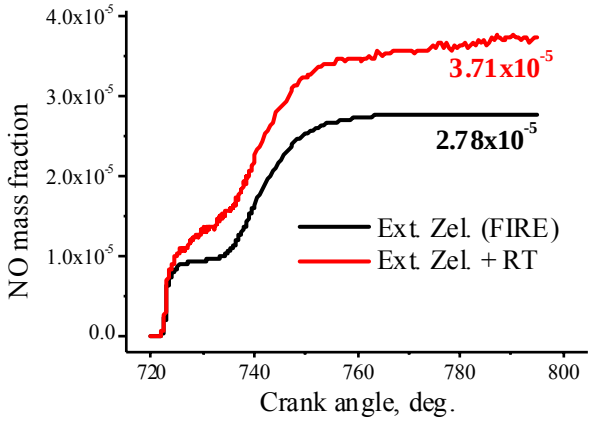

Figure 5. Time histories of thermal NO emissions predicted by the standard ECFM-3Z + Extended Zel'dovich NO model (black curve) and ECFM-3Z + Extended Zel'dovich NO + RT-model (red curve) for the operation point #5794 of Diesel engine.

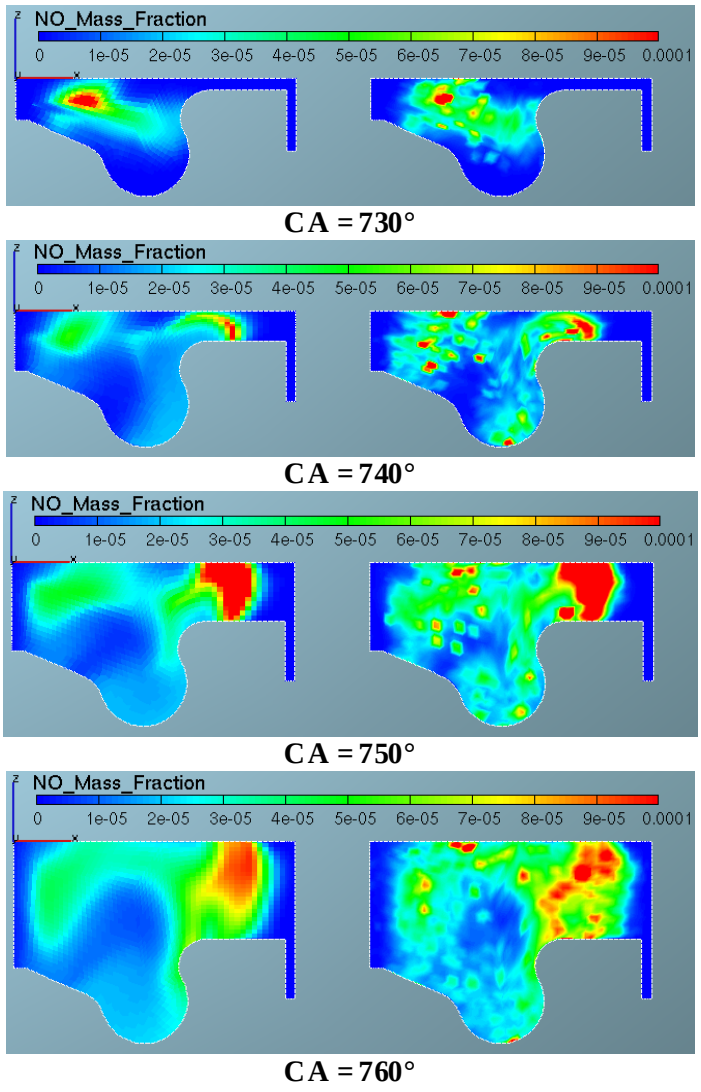

Figure 6. Spatial distributions of NOx mass fraction in the engine at different values of crank angle for the operation point 5794 of Diesel engine using the settings provided by AVL. Left: standard ECFM-3Z + Extended Zel'dovich FIRE model, Right: RT-model.

the engine flow field, we have plotted the probability density functions (PDFs) of residence times of notional elements in three different spherical regions of the computational domain. The characteristic diameter of each region was taken equal to 2 mm. Figure 7 shows the approximate location of these regions in the combustion chamber. Note that all the regions were located at the grid angle bisector, i.e., in the central part of the computational domain rather than at its boundaries. The first region is located not far from the fuel injection point (there are strong recirculation flows in this region). The second region is located at the border of the fuel spray and corresponds approximately to the location where mixture autoignition occurs. The third region is located in that part of the combustion chamber where the maximum concentration of NO is observed in the calculations (see Fig. 6).

Figure 8 shows the predicted PDFs of residence times of notional elements in all three regions (red curves). These PDFs were plotted based on the statistics of about 40,000 notional elements flying through the regions during the entire computation time. Also shown in Figure 8 are the PDFs of element residence times calculated based on solely mean flow velocity provided by AVL FIRE (black curves). It is seen that the peak values for the black curves (based on the element mean velocity) are, as a rule, higher than for the red curves (based on the mean + pulsating element velocity). Also, the red curves appear to be wider than the black curves, i.e. when considering velocity fluctuations, longer residence times are getting more likely. Mo

Calculations of soot formation

The RT-model was also applied to the simulation of soot formation. Figure 9 compares the cumulated soot mass fractions obtained for 14 operation points using the Kinetic soot model and the Kinetic soot model coupled with the RT-model. Clearly, for all operation points the RT-model provides somewhat higher soot emissions.

Figure 10 compares the time histories of cumulated soot mass fraction in engine cylinder for the Kinetic soot model (black curve) and for that combined with the RT-model (red curve) for the operation point #5794.

The differences in the models under consideration are demonstrated in Fig. 11 depicting the spatial distributions of soot mass fractions at different CA. The left and right figures correspond to the Kinetic soot model and to the Kinetic model combined with the RT-model, respectively. As seen, the RT-model is capable of resolving local regions with relatively large soot mass fracrtions caused by large residence times in fuel-rich recirculation zones.

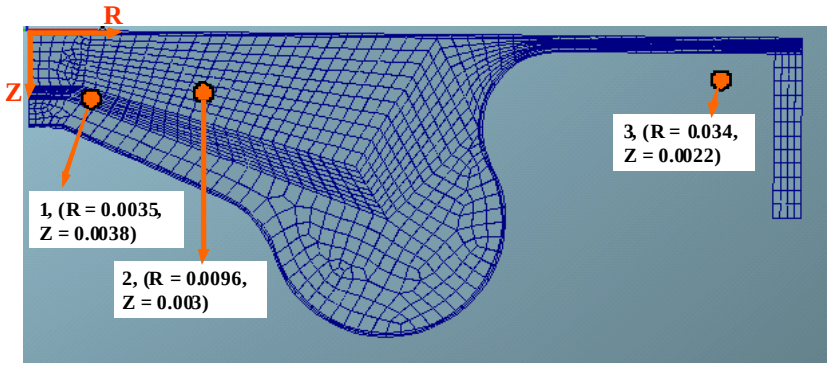

Figure 7. Location of the regions where the probability density functions of residence times of notional particles are monitored.

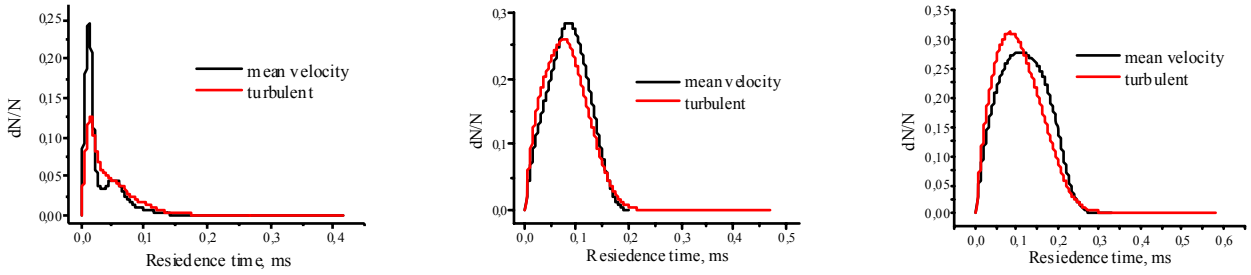

Region 1 **Region 2** **Region 3**

Figure 8. Predicted PDFs of residence times of notional elements in three regions 1 to 3 for the operation point #5794 of Diesel engine. Red curves correspond to the RT-model taking into account both mean and turbulent element velocity. Black curves take into account only mean element velocity.

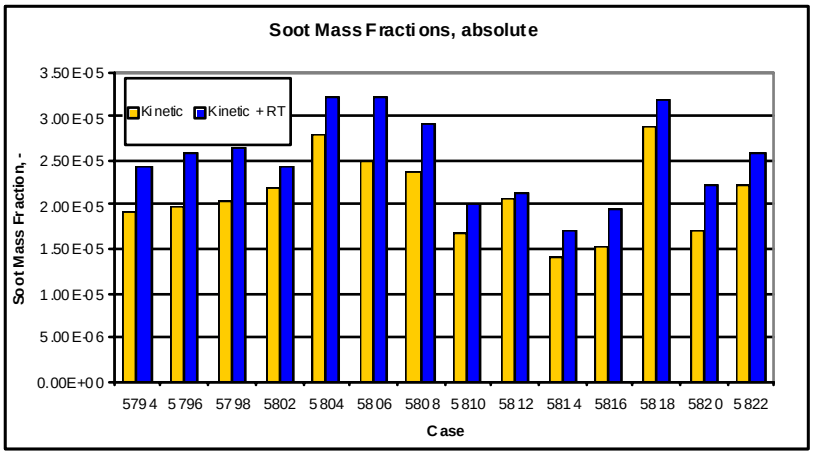

Figure 9. Comparison of soot emissions predicted by the standard ECFM-3Z + Kinetic soot model (left columns marked in yellow) and the RT-model for different operation points of Diesel engine (right columns marked in blue).

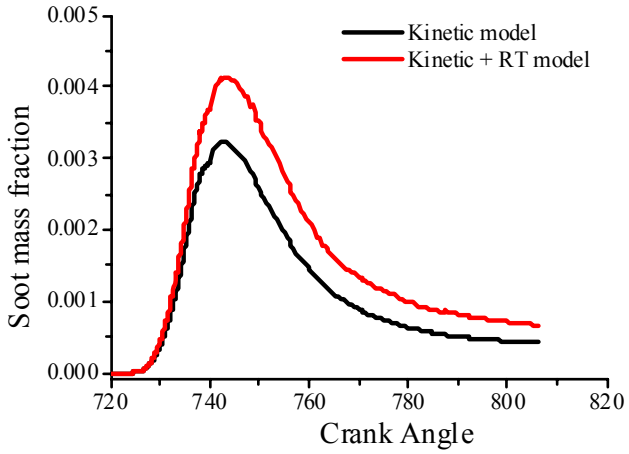

Figure 10. Time histories of soot emissions predicted by the standard soot model (black curve) and standard soot + RT-model (red curve) for the operation point #5794 of Diesel engine.

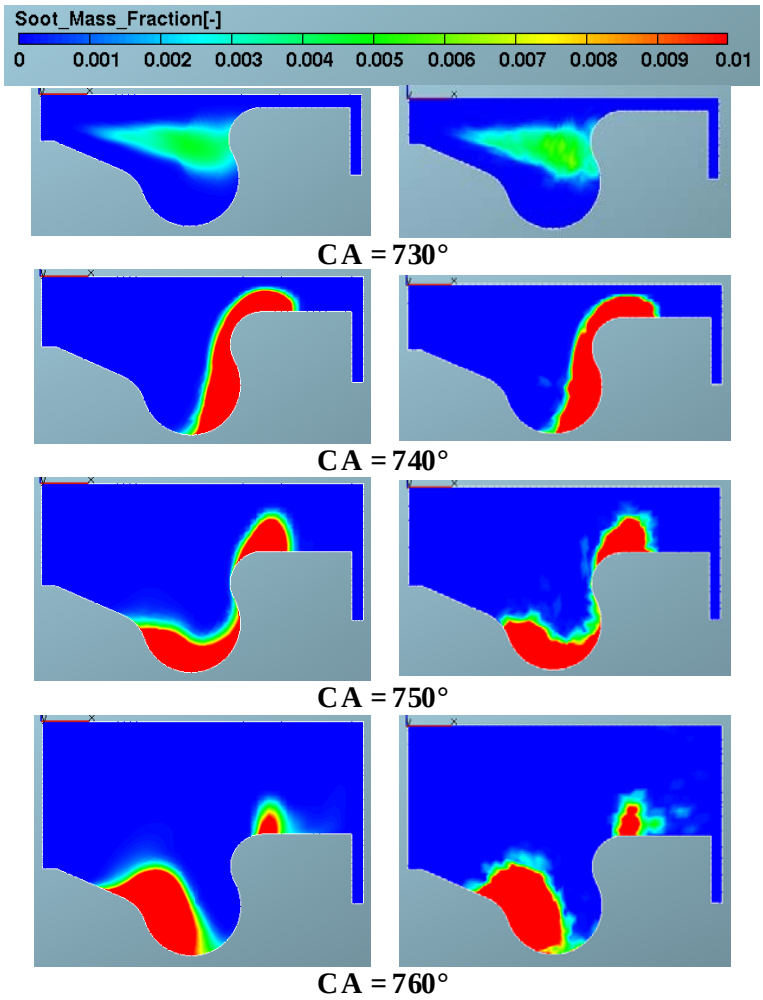

Figure 11. Spatial distributions of soot mass fraction in Diesel engine at different values of crank angle for the operation point #5794. Left: Kinetic soot model; Right: Kinetic + RT model.

CONCLUSIONS

The new simple and computationally efficient method of predicting pollutant formation in IC engines with due regard for residence time distribution in computational cells has been developed and tested.

The method is based on tracing multiple fluid elements in the turbulent flow field. Mathematically it implies the solution of motion equations for the elements and calculation of pollutants formation in those elements using the reaction rates provided by any available model. The resultant rate of pollutant formation in a computational cell is found by averaging over all elements in cell, thus taking into account the wide spectrum of residence time in the cell.

The method intrinsically provides better physical representation of the conditions in the combustion chamber and improves the predictions of pollutant (NO and soot) emissions.

ACKNOWLEDGMENTS

This work was partly supported by AVL LIST GmbH, Russian Foundation for Basic Research, and State contract of Russian Federation # П502.

REFERENCES

Pope, S.B., 1985, "PDF Methods for turbulent reactive flows", *Prog. Energy Combust. Sci.*, 11, 119.

FIRE v2010 Manual, 2010, AVL List GmbH, Graz.

Priesching, P., Ramusch, G., Ruetz, J., Tatschl, R., 2007, "3D-CFD Modeling of Conventional and Alternative Diesel Combustion and Pollutant Formation – A Validation Study." SAE Paper 2007-01-1907.

Bowman, C. T., 1992, "Control of Combustion-Generated Nitrogen Oxide Emissions: Technology Driven by Regulation", *Proc. Twenty-Fourth Symposium (International) on Combustion*, The Combustion Institute, Pittsburgh, PA, 859-878.

Hill, S.C., Smoot, L. D., 2000, "Modeling of Nitrogen Oxides Formation and Destruction in Combustion Systems", *Progress in Energy and Combustion Science*, 26, 417-458.

De Soete, G. G., 1975, "Overall Reaction Rates of NO and N2 Formation from Fuel Nitrogen, *Proc. 15th Symposium (International) on Combustion*, The Combustion Institute, Pittsburgh, 1093.

Frolov, S.M., Basevich, V.Ya., Vlasov, P.A., Skripnik, A.A., Priesching, P., Tatschl, R., 2007, "Modeling of Soot Formation in Internal Combustion Engines," *Proc. Int. Conf. "Engine-2007,"* Moscow, Bauman State University, 28-37.

Ackermann, J., Wulkow, M., 1990, "MACRON–A Program Package for Macromolecular Kinetics," Preprint SC 90-14, Konrad-Zuse-Zentrum, Berlin.

Vlasov, P.A., Warnatz, J., 2002, "Detailed Kinetic Modeling of Soot Formation in Hydrocarbon Pyrolysis behind Shock Waves," *Proc. Combust. Inst.*, 29, 2335–2341.

Deuflhard, P., Wulkow, M., 1989, "Impact of Computing in Science and Engineering," 1, 269 –301.